Research Article | Vol. 25, No. 24 | 27 Nov 2017 | OPTICS EXPRESS 30764
Optics EXPRESS

Liquid-crystal tunable color filters based on aluminum metasurfaces

ZU-WEN XIE,[1] JHEN-HONG YANG,[2] VISHAL VASHISTHA,[3] WEI LEE,[4] AND KUO-PING CHEN[4,*]

[1]*Institute of Lighting and Energy Photonics, National Chiao Tung University, Guiren Dist, Tainan 71150, Taiwan*
[2]*Institute of Photonic System, National Chiao Tung University, Guiren Dist., Tainan 711, Taiwan*
[3]*Faculty of Physics, Adam Mickiewicz University in Poznan, Poland*
[4]*Institute of Imaging and Biomedical Photonics, National Chiao Tung University, Guiren Dist., Tainan 71150, Taiwan*
[*]*kpchen@nctu.edu.tw*

Abstract: Designing color pixels using plasmonic nanostructures and metasurfaces has become a luring area of research in recent years. Here, we experimentally demonstrated the voltage tunability of a dynamic plasmonic color filter by using an aluminum grating integrated with the nematic liquid crystal (LC). Along with a typical substrate coated with rubbed polyimide film, the aluminum grating itself serves as a molecular alignment layer to form a twisted LC cell. This hybrid structure allows electrically controlled transmission color by applying the voltage. A significant spectral tunability of such a device has been demonstrated by applying the small voltage from 0 to 4 V_{rms}.

OCIS codes: (250.5403) Plasmonics; (160.3918) Metamaterials; (230.3720) Liquid-crystal devices.

References and links

1. A. Kristensen, J. K. Yang, S. I. Bozhevolnyi, S. Link, P. Nordlander, N. J. Halas, and N. A. Mortensen, "Plasmonic colour generation," Nat. Rev. Mater. **2**, 16088 (2016).
2. N. Dean, "Colouring at the nanoscale," Nat. Nanotechnol. **10**(1), 15–16 (2015).
3. X. Zhu, W. Yan, U. Levy, N. A. Mortensen, and A. Kristensen, "Resonant laser printing of structural colors on high-index dielectric metasurfaces," Sci. Adv. **3**(5), e1602487 (2017).
4. V. Raj Shrestha, S.-S. Lee, E.-S. Kim, and D.-Y. Choi, "Polarization-tuned dynamic color filters incorporating a dielectric-loaded aluminum nanowire array," Sci. Rep. **5**, 12450 (2015).
5. C.-W. Su and K.-P. Chen, "Broadband gold nanoantennas arrays with transverse dimension effects," Opt. Express **24**(16), 17760–17765 (2016).
6. T. D. James, P. Mulvaney, and A. Roberts, "The plasmonic pixel: large area, wide gamut color reproduction using aluminum nanostructures," Nano Lett. **16**(6), 3817–3823 (2016).
7. F. Cheng, J. Gao, T. S. Luk, and X. Yang, "Structural color printing based on plasmonic metasurfaces of perfect light absorption," Sci. Rep. **5**, 11045 (2015).
8. Z. Li, A. W. Clark, and J. M. Cooper, "Dual Color Plasmonic Pixels Create a Polarization Controlled Nano Color Palette," ACS Nano **10**(1), 492–498 (2016).
9. K. Diest, J. A. Dionne, M. Spain, and H. A. Atwater, "Tunable Color Filters Based on Metal-Insulator-Metal Resonators," Nano Lett. **9**(7), 2579–2583 (2009).
10. M. Miyata, H. Hatada, and J. Takahara, "Full-color subwavelength printing with gap-plasmonic optical antennas," Nano Lett. **16**(5), 3166–3172 (2016).
11. V. Vashistha, G. Vaidya, R. S. Hegde, A. E. Serebryannikov, N. Bonod, and M. Krawczyk, "All-Dielectric Metasurfaces Based on Cross-Shaped Resonators for Color Pixels with Extended Gamut," ACS Photonics **4**, 1076–1082 (2017).
12. X. Zhu, C. Vannahme, E. Højlund-Nielsen, N. A. Mortensen, and A. Kristensen, "Plasmonic colour laser printing," Nat. Nanotechnol. **11**(4), 325–329 (2016).
13. V. Vashistha, G. Vaidya, P. Gruszecki, A. E. Serebryannikov, and M. Krawczyk, "Polarization tunable all-dielectric color filters based on cross-shaped Si nanoantennas," Sci. Rep. **7**(1), 8092 (2017).
14. W. Yue, S. Gao, S. S. Lee, E. S. Kim, and D. Y. Choi, "Highly reflective subtractive color filters capitalizing on a silicon metasurface integrated with nanostructured aluminum mirrors," Laser Photonics Rev. **11**, 1600285 (2017).
15. T. Ellenbogen, K. Seo, and K. B. Crozier, "Chromatic plasmonic polarizers for active visible color filtering and polarimetry," Nano Lett. **12**(2), 1026–1031 (2012).
16. Y.-W. Huang, W. T. Chen, W.-Y. Tsai, P. C. Wu, C.-M. Wang, G. Sun, and D. P. Tsai, "Aluminum plasmonic multicolor meta-hologram," Nano Lett. **15**(5), 3122–3127 (2015).

#307765 https://doi.org/10.1364/OE.25.030764
Journal © 2017 Received 28 Sep 2017; revised 15 Nov 2017; accepted 18 Nov 2017; published 22 Nov 2017

Optics EXPRESS

17. J.-H. Yang and K.-P. Chen, "Evanescent Wave-Assisted Symmetry Breaking of Gold Dipolar Nanoantennas," Sci. Rep. **6**, 32194 (2016).
18. X. Duan, S. Kamin, and N. Liu, "Dynamic plasmonic colour display," Nat. Commun. **8**, 14606 (2017).
19. M. L. Tseng, J. Yang, M. Semmlinger, C. Zhang, P. Nordlander, and N. J. Halas, "Two-Dimensional Active Tuning of an Aluminum Plasmonic Array for Full-Spectrum Response," Nano Lett. **17**(10), 6034–6039 (2017).
20. M. W. Knight, N. S. King, L. Liu, H. O. Everitt, P. Nordlander, and N. J. Halas, "Aluminum for plasmonics," ACS Nano **8**(1), 834–840 (2014).
21. J. Olson, A. Manjavacas, T. Basu, D. Huang, A. E. Schlather, B. Zheng, N. J. Halas, P. Nordlander, and S. Link, "High chromaticity aluminum plasmonic pixels for active liquid crystal displays," ACS Nano **10**(1), 1108–1117 (2016).
22. W. Dickson, G. A. Wurtz, P. R. Evans, R. J. Pollard, and A. V. Zayats, "Electronically controlled surface plasmon dispersion and optical transmission through metallic hole arrays using liquid crystal," Nano Lett. **8**(1), 281–286 (2008).
23. V. K. Hsiao, Y. B. Zheng, B. K. Juluri, and T. J. Huang, "Light-driven plasmonic switches based on au nanodisk arrays and photoresponsive liquid crystals," Adv. Mater. **20**, 3528–3532 (2008).
24. G. Si, Y. Zhao, E. S. P. Leong, and Y. J. Liu, "Liquid-crystal-enabled active plasmonics: a review," Materials (Basel) **7**(2), 1296–1317 (2014).
25. Y.-C. Hsiao, C.-W. Su, Z.-H. Yang, Y. I. Cheypesh, J.-H. Yang, V. Y. Reshetnyak, K.-P. Chen, and W. Lee, "Electrically active nanoantenna array enabled by varying the molecular orientation of an interfaced liquid crystal," RSC Advances **6**, 84500–84504 (2016).
26. K.-P. Chen, S.-C. Ye, C.-Y. Yang, Z.-H. Yang, W. Lee, and M.-G. Sun, "Electrically tunable transmission of gold binary-grating metasurfaces integrated with liquid crystals," Opt. Express **24**(15), 16815–16821 (2016).
27. G. Gilardi, D. Donisi, A. Serpengüzel, and R. Beccherelli, "Liquid-crystal tunable filter based on sapphire microspheres," Opt. Lett. **34**(21), 3253–3255 (2009).
28. A. Komar, Z. Fang, J. Bohn, J. Sautter, M. Decker, A. Miroshnichenko, T. Pertsch, I. Brener, Y. S. Kivshar, and I. Staude, "Electrically tunable all-dielectric optical metasurfaces based on liquid crystals," Appl. Phys. Lett. **110**, 071109 (2017).
29. Y. J. Liu, G. Y. Si, E. S. Leong, N. Xiang, A. J. Danner, and J. H. Teng, "Light-driven plasmonic color filters by overlaying photoresponsive liquid crystals on gold annular aperture arrays," Adv. Mater. **24**(23), OP131–OP135 (2012).
30. D. Franklin, Y. Chen, A. Vazquez-Guardado, S. Modak, J. Boroumand, D. Xu, S.-T. Wu, and D. Chanda, "Polarization-independent actively tunable colour generation on imprinted plasmonic surfaces," Nat. Commun. **6**, 7337 (2015).
31. W. Lee, J.-S. Gau, and H.-Y. Chen, "Electro-optical properties of planar nematic cells impregnated with carbon nanosolids," Appl. Phys. B **81**, 171–175 (2005).
32. G. Bryan-Brown, C. Brown, I. Sage, and V. Hui, "Voltage-dependent anchoring of a nematic liquid crystal on a grating surface," Nature **392**, 365–367 (1998).
33. S. P. Palto, M. I. Barnik, V. V. Artemov, I. V. Kasyanova, N. M. Shtykov, A. R. Geivandov, S. G. Yudin, and M. V. Gorkunov, "Voltage-tunable optical transmission of subwavelength metal gratings filled with liquid crystals," in *SPIE Photonics Europe* (International Society for Optics and Photonics, 2016), 988307–988307–988308.
34. Q. Cao and P. Lalanne, "Negative role of surface plasmons in the transmission of metallic gratings with very narrow slits," Phys. Rev. Lett. **88**(5), 057403 (2002).

1. Introduction

Color filtering is a key function in many optical and optoelectronics applications such as camera, projector, CMOS image sensors, and many imaging and hand-held devices. Recent developments in plasmonics-based structural color filters can be expected as possible replacement of pigment-based color printing in the future. The structural color filter exhibits significant advantages over existing pigment-based technology, such as being compact in size, rendering non-degradable colors, having resolution well below the diffraction limit, and being environmentally friendly [1, 2]. The new technique of developing structural color devices based on femtosecond laser gives a new direction for the possibility of mass production [3].

Different approaches have been suggested to show the capability of structure-based color filtering, including metallic grating structures [4, 5], metallic disks [1, 6], complementary metallic design [7, 8], metal–insulator–metal (MIM) structures [9, 10], all-dielectric [3, 11–13], and hybrid structures [4, 14]. However, the main challenge is to design a tunable color filter. The capability of a structural color filter is limited owing to the fact that the response of the color filter is fixed once the device is fabricated. Recently, some research groups have demonstrated significant tunability of structural color filters by various means. A non-symmetric structure approach is used to tune the response based on polarization of incident

Optics EXPRESS

light [8, 13, 15, 16]. Unfortunately, the tunability range of these devices is quite narrow, and it is very difficult to fabricate such structures. Other popular approaches rely on anti-bonding mode resonances [17] or MIM resonators [9] to tune the resonance wavelengths, but the size of the MIM-based devices are in the micron range, which is difficult to integrate with chips. It is obvious that tunable color filtering is still an open area of research. According to the literature, a couple of new techniques have been disclosed for tuning the color by means of hydrogen-responsive Mg nanoparticles [18] and mechanically stretchable substrates as active metasurfaces in dynamic plasmonic color display [19].

In this paper, we integrated the nematic liquid crystal (LC) with a simple aluminum (Al) grating metasurface. The cell thus formed shows significant spectral tunability by applying various voltages across the cell thickness. The reason to choose Al is its low interband transition loss, which can provide more vivid colors [20, 21]. LC has already been used to design active nanophotonics devices [22–25], beam-steering [26], tunable filters with microspheres [27], and phase-controlled all-dielectric metasurface [28] to achieve the tunability of resonance at near-infrared (NIR) wavelengths. An earlier attempt has also been made to enable the tunability of resonance in the visible range [29, 30]. However, the tunable color filter using aluminum metasurface in the visible range is less studied, in particular with the transmission mode. The working principle of our device is based on the fact that LC possesses both dielectric anisotropy and optical anisotropy, consequently exhibiting polarization tunability when a small electric field is applied across the LC. This anisotropic behavior can be easily manifested in a cell with twisted alignment of the LC. In a typical twisted-nematic cell, an applied voltage imposes an electric torque on the LC molecules against the restoring elastic one, causing the molecular axis and, in turn, the optic axis of the LC to tilt toward the field direction. The tilted optic axis thus results in the change in effective refractive index. We utilized the anisotropic property of LC combined with an Al grating metasurface to realize the tunability of color filter.

2. Sample Fabrication

The Al grating metasurfaces were fabricated using electron-beam lithography (EBL). To define a pattern, polymethylmethacrylate (PMMA) of 200 nm in thickness was coated on a typical indium–tin-oxide (ITO)-coated glass substrate followed by a patterning process. A 90 nm thin film of Al was deposited by using the E-gun evaporator. The Al gratings would be formed by lift-off process and they have the desired effect to align the contacting LC molecules to lie perpendicularly to the grating vector in the metasurface plane.

The ITO glass substrate with an Al grating metasurface serves as the bottom plate of the LC cell. The top plate of the cell is ITO glass spin-coated with a mechanically buffed polyimide layer for planar alignment of the LC molecules. The rubbing direction is parallel to the grating vector when assembled with a cell gap of 5 μm. The nematic liquid crystal E7, with extraordinary refractive index n_e = 1.7472 and ordinary refractive index n_o = 1.5217 at the temperature of 20 °C and wavelength of 589.3 nm, was introduced into each empty cell by capillary action. An alternating current (AC) voltage (1 kHz) was applied across the cell gap through ITO layers to control the state of LC. The schematic of the cell configuration is shown in Fig. 1. At null voltage, the polarization direction of linearly polarized light of normal incidence rotates by 90° after emerging from the cell through the polarization-rotation effect [31] in a twisted nematic cell as shown in Fig. 1(a). In Fig. 1(b), by increasing the voltage to unwind the twist and maximize the tilt in the LC bulk, the polarization of linearly polarized light remains virtually unchanged, in perpendicular to the grating vector.

Optics EXPRESS

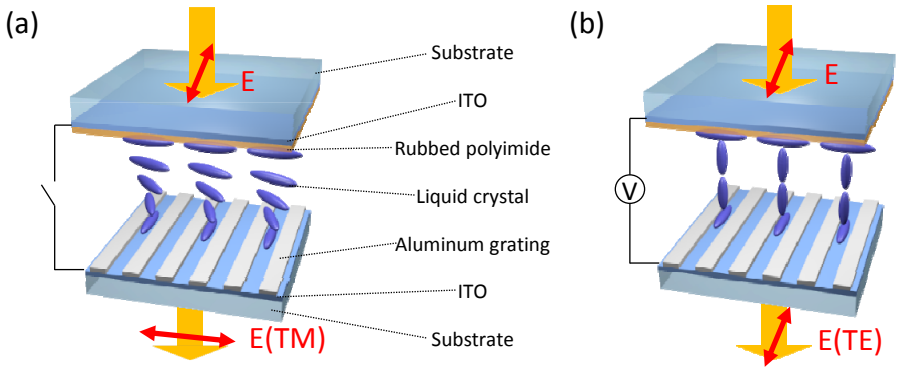

Fig. 1. Schematic of the cell composed of sandwiched nematic LC, an Al grating and a polyimide-coated substrate in the (a) voltage-off and (b) voltage-on states.

3. Spectral Characterization of Metasurfaces

For this work, the grating structures were designed with a fixed duty ratio of 0.5 and with three distinct widths: 150 nm, 200 nm and 230 nm. Figure 2(a) schematically depicts the design of a parallel-stripe-patterned grating characterized by the height *h*, width *w* and period (or grating constant) P (P = 2w) . Figure 2(b) shows a scanning electron microscope (SEM) image of one fabricated grating sample having h = 90 nm, w = 150 nm and P = 300 nm.

Transmission spectra of each grating were then recorded for both TE and TM cases. All the collected data were normalized with respect to the bare ITO-coated glass substrate. A camera was used to take the micrographs of the illuminated area. Figures 2(c)–2(e) show the comparisons of simulated and experimental spectra of the TM mode for three different grating structures. Note that the three insets show the correspondingly observed colors in transmission. Similar measurements were carried out for TE polarized light as shown in Figs. 2(f)–2(h). The experimental spectra are in reasonable agreement with simulated data.

From Figs. 2(c)–2(e), it is clear that there are pronounced changes in the three transmission spectra for TM polarization so the change in color is dramatic and vivid. In contrast, the TE polarization produces featureless-like spectra, giving rise to limited change in color as shown in Figs. 2(f)–2(h).

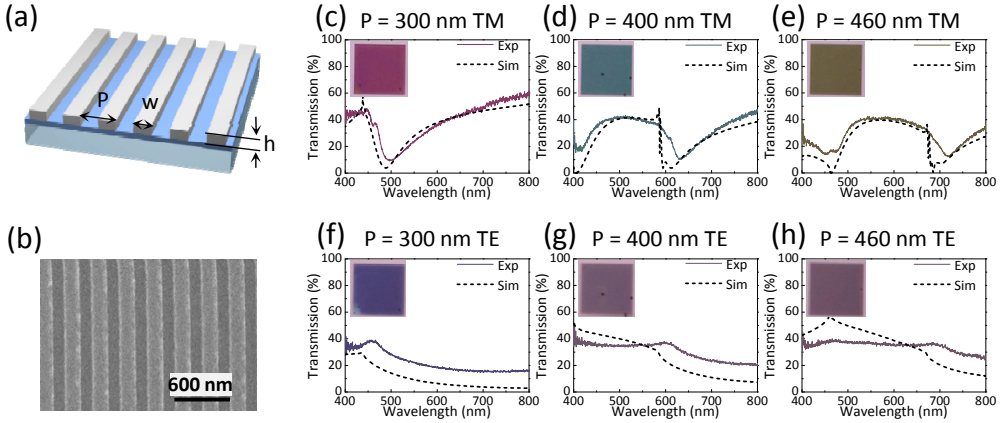

Fig. 2. (a) Schematic of the Al grating on the ITO coated glass substrate. (b) SEM image of aluminum grating with grating width 150 nm. The simulated and experiment transmission spectra of the aluminum grating when the incident light is (c)-(e) TM polarization and (f)-(h) TE polarization. The insets show the images directly recorded by optical microscopy with a camera.

Optics EXPRESS

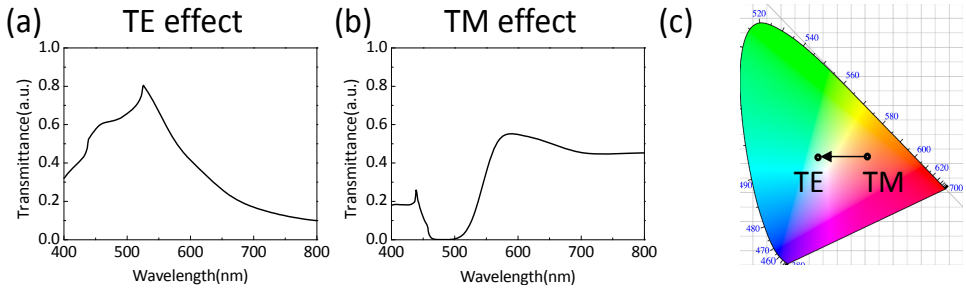

Fig. 3. Simulated transmission spectra of an Al grating integrated with LC for P = 300 nm: (a) TE polarization; (b) TM polarization. (c) Change in color from TM to TE polarization as indicated by the color space coordinates on the CIE-1931 chromaticity diagram.

4. Modeling

In order to fit the experimental observation, simulations were performed by using finite difference time domain (FDTD) method, (FDTD Solutions, Lumerical). In the modeling, the LC molecules around the grating slits are parallel to the grating [32]. Therefore, for TE polarization, the vibration direction of incident optical electric field will be parallel to the molecular of the liquid crystal, and the effective refractive index of LC is n_e = 1.75. On the other hand, for the TM case, the vibration direction of electric field will be perpendicular to the molecular axis of the LC in the bulk, and the effective refractive index is n_o = 1.52.

Figure 3 shows the transmittance spectra of TE and TM polarizations with LC. By comparing Figs. 2(f) and 3(a), the resonance peak in the transmittance spectrum of TE polarization with LC is much higher and sharper than that of in air, so the color will be vivid in LC. In Fig. 3(a), the resonance peaks around 438 nm and 525 nm are diffraction signals given by [33]

$$\lambda = Pn_i, \tag{1}$$

where, P = 300 nm is the period of the grating and n_i is the refractive index of the surrounding medium of the grating. In TE polarization, the prime effect is diffraction and waveguide mode resonance [34], so the extraordinary transmission peaks in Fig. 3(a) would be influenced by the refractive index of the surrounding medium. Since the refractive indices of the substrate n_{sub} = 1.46 and of the LC $n_{LC} = n_e = 1.75$, there are two peaks at 438 nm and 525 nm. On the other hand, if the refractive index of substrates and liquid crystals could match, the narrower transmission band could be achieved.

In Fig. 3(b), the broad band resonance dip spanning from 460 nm to 484 nm is due to the plasmon resonance for TM polarization [34], which is given by [33]

$$\lambda = p\sqrt{\frac{\varepsilon_m \varepsilon_i}{\varepsilon_m + \varepsilon_i}}, \tag{2}$$

where ε_m and ε_i are dielectric permittivity of metal and surrounding medium, respectively. In TM polarization, the transmittance is near zero from 460 nm to 484 nm because the grating structures would provide the extra k-vector to excite surface plasmon polaritons [34]. We observed two resonance dips at 460 nm and 484 nm corresponding to the substrate ($\varepsilon_i \cong 1.46^2$) and the LC ($\varepsilon_i \cong (n_0)^2 = 1.52^2$). However, the two resonance wavelengths are close to each other, so the two resonance dips coalesce together to form a broadband resonance dip. A

Optics EXPRESS

CIE-1931 chromaticity diagram is shown in Fig. 3(c) to help visualize the switch of color from TM to TE polarization.

5. Tunability of Colors

Figure 4 shows the experimental results of Al gratings integrated with LC. The polarization direction of incident light is parallel to the grating stripes. When the applied voltage is 0 V, the polarization direction of electric field on the Al grating is twisted by 90° and changed to become parallel to the grating vector through the LC bulk. Because of the unperturbed twisted-nematic state of LC configuration, the TM polarization effect could be achieved when the applied voltage is 0 V in this framework. In contrast, the TE polarization effect could be achieved when the applied voltage is higher than 4 V_{rms} because the LC molecules are reoriented vertically to the substrate by the externally applied voltage across the cell thickness to permit the polarization state of light uninfluenced or untwisted in the passage through the cell. This is the key to enabling active tuning of color in our device.

By changing the state of LC using a small applied voltage, the color changed along with the TE and TM polarizations. The variations in color and spectrum with increasing voltage for two different grating constants are shown in Figs. 4(a) and 4(b). One can see that, with a small applied voltage, the spectrum and, in turn, color of the cells can be varied. The change from the corresponding the TM mode at 0 V to the TE mode at 4 V_{rms} thus provides dynamic color tunability. In Fig. 4(c), the gradual color variation is demonstrated with the applied voltage from 2 V_{rms} to 4 V_{rms}. When the applied voltage is larger than 4 V_{rms}, the color would fix, because the molecules of LC are untwisted and totally aligned vertically.

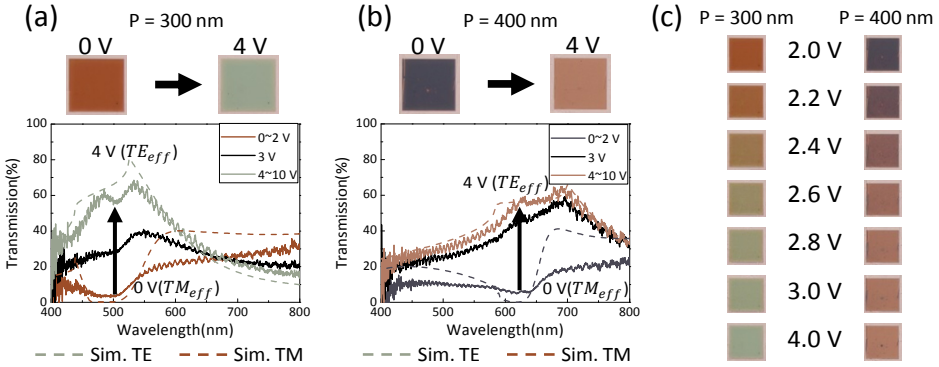

Fig. 4. Experiment results of LC cells with Al gratings when the applied voltage increases from 0 V to 10 V_{rms}. The images on the top of spectral are optical images recorded by a CCD camera: (a) P = 300 nm (b) P = 400 nm. (c) Transmissive color appearance of the cells at various applied voltages.

6. Conclusion

In conclusion, we have demonstrated a LC-based tunable color filter, which shows high dynamic tunability of color in transmission. The integration of LC with a grating structure allows the broad dynamic tunability in quite controllable manner. By slightly adjusting the applied voltage between 2 V_{rms} and 4 V_{rms}, the color spectra changed in a reasonably broad spectral range. The concept can be extended for integrating LC with plasmonics or all dielectric metasurface-based color filters to achieve the high quality of color pixels. The integration of LC with color filters opens a new possibility to make tunable color filter devices.

Funding

Ministry of Science and Technology, Taiwan, ROC (MOST 104-2221-E-009-130-MY3, 105-2221-E-009-096-MY2, and 106-3114-E-009-004). National Science Centre Poland for

Optics EXPRESS

OPUS grant No. 2015/17/B/ST3/00118 (Metasel). European Union Horizon2020 research and innovation program under the Marie Skłodowska-Curie grant agreement No. 644348 (MagIC).

Acknowledgment

We would like to thank Dr. Shie-Chang Jeng for kindly supplying the liquid crystal used in the study.